International Journal of Environmental Research (2018) 12:45–57
https://doi.org/10.1007/s41742-018-0067-1

RESEARCH PAPER

Physical Adsorption of Horseradish Peroxidase on Reduced Graphene Oxide Nanosheets Functionalized by Amine: A Good System for Biodegradation of High Phenol Concentration in Wastewater

Monireh Besharati Vineh[1] · Ali Akbar Saboury[2] · Amir Ali Poostchi[3] · Leila Mamani[4]

Received: 25 September 2017 / Revised: 1 December 2017 / Accepted: 2 January 2018 / Published online: 20 January 2018

Abstract

The activity and pH/thermal/storage stability have been investigated for Horseradish peroxidase (HRP) physically immobilized onto modified reduced graphene oxide ($RGO{\cdot}NH_2$) nanoparticles (NPs) and compared to the free enzyme. The NPs were synthesized with a size of about 70 nm and functionalized to have amine groups. The NPs, free and immobilized HRP were characterized using Fourier transform infrared spectra, scanning electron microscopy, zeta potential measurement, and UV/visible spectroscopy. The results obtained from activity assays showed that the catalytic constant, k_{cat}, value became more than sixfold and the catalytic efficiency, k_{cat}/K_m, value increased about sevenfold after immobilization. The results also indicated that the catalytic activity reached 133-fold (for 2 mg mL^{-1} of NPs) and 120-fold (for 1.5 mg mL^{-1} of NPs) when HRP was immobilized. The optimum pH was also obtained at 7.0 for both free and immobilized HRP. At 50 °C, the immobilized HRP retained 75% of the initial activity, while 60% initial activity remained for the free HRP after 120 min. The excellent reusability of immobilized HRP was also observed and the activity retained about 60% of the first use after ten cycles. The results also revealed that the activities reached 50% of initial activity for the immobilized HRP when the samples were stored for 35 days. The data obtained from circular dichroism spectroscopy displayed that the α-helical content of the enzyme was decreased after immobilization. The removal efficiency for high concentration phenol (2500 mg L^{-1}) was 100 and 53% for the immobilized HRP and free HRP, respectively.

Keywords Horseradish peroxidase · Physical adsorption · Reduced graphene oxide · Activity improvement · Phenol biodegradation

Abbreviation

HRP	Horseradish peroxidase
NPs	Nanoparticles
GO	Graphene oxide
RGO	Reduced graphene oxide
$RGO{\cdot}NH_2$	Modified reduced graphene oxide
$RGO{\cdot}NH_2$@HRP	Reduced graphene oxide·NH_2@ horseradish peroxidase
4-AAP	4-Aminoantipyrine
H_2O_2	Hydrogen peroxide
DW	Deionized water
SEM	Scanning electron microscopy
FT-IR	Fourier transform infrared spectroscopy

✉ Ali Akbar Saboury
saboury@ut.ac.ir

1 Department of Biology, Science and Research Branch, Islamic Azad University, Tehran, Iran

2 Institute of Biochemistry and Biophysics, University of Tehran, Tehran, Iran

3 Petrochemical Industries Development Management Company, P.O. Box 15858-49568, Tehran, Iran

4 Department of Nanotechnology, Agricultural Biotechnology Research Institute of Iran (ABRII), Agricultural Research, Education and Extension Organization (AREEO), Karaj, Iran

Introduction

Horseradish peroxidase (HRP; EC 1.11.1.7) is an oxidoreductase enzyme that oxidizes a variety of organic and inorganic compounds (Khurshid et al. 2012). Peroxidase is produced from different sources such as animals, plants, and microbes. The HRP applied in this research was a member of the plant peroxidase superfamily extracted from horseradish roots (*Armoracia rusticana*). As can be seen in

Eq. 1, the HRP is normally applied to catalyze the oxidation reaction of substrates such as phenols and aromatic amines using H_2O_2 as an oxidant agent (Feng et al. 2015; Lavery et al. 2010; Mogharrab et al. 2007; Sun et al. 2004; Zhang et al. 2014). Reaction catalyzed by HRP is given in the following equation:

$$\text{Substrate}_{(\text{reduced})} + H_2O_2 \overset{\text{HRP}}{\rightarrow} \text{Substrate}_{(\text{oxidized})} + H_2O. \quad (1)$$

Aromatic compounds including phenol, cresol, chlorophenols, chlorinated phenols, and aromatic amines were classified as dangerous and resistant pollutants (Bansal and Kanwar 2013). These compounds threaten human health with cancer and fetal mutation and the life of marine creatures. To purify the waste streams containing phenolic compounds, several treatment processes including physical, chemical, and biological were proposed by researchers (Gómez et al. 2006; Pradeep et al. 2015; Tavakoli et al. 2017). These treatment methods were often not suitable due to high installation and operation cost, long treatment time, low efficiency, and the production of hazardous by-products. The enzymatic treatment method by various herbal sources using peroxidase enzymes could be considered as an effective approach to convert the waste streams into the harmless by-products (Gómez et al. 2006; Pradeep et al. 2015).

Due to the instability of the free enzymes under normal operational conditions, the immobilization of the enzymes could be applied to reserve the stability of the enzymes, thus minimizing the operational cost significantly (Xu et al. 2013). Nanoparticles (NPs) were well known as an effective support for enzyme immobilization because of their high surface area, high loading capacity, and high diffusion efficiency. To select the nanoscale materials, the aspects of human protection and environment regulations should be considered (Chang and Tang 2014; Zhang et al. 2015).

In the previous studies, to remove the wide range of the pollutants, HRP was immobilized on nanoparticles such as chitosan–halloysite hybrid-nanotubes (Zhai et al. 2013), silica nanoparticles, hydrous-titanium (Ai et al. 2016), graphene oxide/Fe_3O_4 (Chang et al. 2016), super paramagnetic Fe_3O_4/graphene oxide (Chang et al. 2015), nanospray dried ethylcellulose particles (Dahili et al. 2015), NH_2-modified magnetic Fe_3O_4/SiO_2 (Chang and Tang 2014), and nanofibrous membranes (Xu et al. 2015). Carbon-based materials such as graphene family have some advantages, including biodegradability, two-dimensional layer structure, large surface area, high pore volume, high stability, and present of surface functional groups on them. These materials have broadly been used for immobilization of enzymes and water purification (Guo and Mei 2014; Kemp et al. 2013). Graphene oxide (GO) and its reduced form (RGO) have some surface oxygen-functional groups such as carboxylic (–COOH), hydroxyl (–OH), and epoxide groups, and are soluble in water and polar organic solvents (Zhang et al. 2013). The HRP has been immobilized on the surface of graphene through hydrophobic effects and π–π interactions, whereas the immobilization of HRP on the surface of GO/RGO has been established through electrostatic interactions and hydrogen bonding owing to their greater amounts of oxygen-containing functional groups (Zhang et al. 2015). Graphene-based nanomaterials could enhance biocatalysts effects of the enzyme. In fact, active oxygen compound generated from endogenous biological processes and exogenous sources had the responsibility for the oxidation of the enzyme and loss of the enzyme activity. RGO could remove hydroxyl and dithiocyanate radicals owing to its property as an antioxidant which protected the enzymes from inactivation. RGO also promoted the stability of the enzyme and acted as a radical quencher (Zhang et al. 2015).

The goal of this research effort was to perform the physical adsorption of HRP on the functionalized RGO for the purposes: (1) to promote the kinetic parameters, the activity, the stability, and reusability of the enzyme; and (2) to eliminate the high concentration of phenol. The RGO has been functionalized with amine functional groups to reinforce the electrostatic interaction between the enzyme and NPs, thereby forming the structure of reduced graphene oxide·NH_2@ horseradish peroxidase (RGO·NH_2@-HRP), namely, bio-nanocomposite. The enzymatic kinetic parameters, activity, stabilities (pH, thermal, and storage), and reusability, have been investigated for the free HRP and the bio-nanocomposite. The capability of free HRP and bio-nanocomposite were then evaluated to degrade the high concentration of phenol (2500 mg L^{-1}). All experiments were performed in triplicate.

Materials and Methods

Materials

HRP, 4-aminoantipyrine (4-AAP), potassium ferricyanide, and phenol were purchased from Sigma, and NaH_2PO_4·H_2O and Hydrogen peroxide (H_2O_2) were supplied from Merck. Deionized water (DW) was generated through a Millipore water purification system. GO was prepared from graphite using modified Hummer's method (Chang et al. 2016).

Synthesis of NPs

Using modified Hummer's method, the GO was prepared from graphite. Briefly, 2 g $KMnO_4$ was added to a mixing

solution of graphite powder (1 g) and 50 mL H_2SO_4 98% in an ice bath. The rate of loading was carefully tuned to prevent a sudden increase of mixture temperature. The reaction mixture was mixed for 2 h at temperature less than 10 °C, followed by another 1 h at 35 °C. Then, the mixture was diluted with DW (50 mL) in an ice bath and the temperature was set below 100 °C. After 1 h, the mixture was further diluted with DW (150 mL). Then, H_2O_2 30% (10 mL) was poured into the mixture. The prepared solid was centrifuged and washed with 5% aq. HCl, and then rinsed for several times with DW to remove the HCl. Finally, the product was dried at 60 °C for 24 h. In a practical method, 1 g of the GO was mixed with 0.2 g of $H_3N^+NHCO_2^-$, grounded using a pestle and mortar at ambient condition. The ground mixture stored in closed vessel was allowed to react at 25 °C for 24 h. Finally, 0.82 g of RGO was produced, yielding 81% based on GO (Chang et al. 2016).

Characterization and Identification

Field emission scanning electron microscopy (SEM) (Nova Nano SEM 430, Netherlands) was utilized to characterize the surface morphology of the RGO·NH_2. The surface functionalities of the RGO·NH_2 were further identified by a Fourier transform infrared spectroscopy (FTIR) (Nicolet FT-IR Spectrometer) in the range of 4000–400 cm^{-1} (Zhang et al. 2010; Xiaoche et al. 2012). Zeta potentials were measured by electrophoretic mobility using Zeta PALS (Zeta Plus-Brookhaven, USA).

Adsorption of HRP

Before using the NPs, the NPs mixed into the DW were placed in the freeze dryer (Alpha 1-2, Christ) and then sonicated. To set the identical conditions for all immobilization experiments, HRP was dissolved in a phosphate buffer (PB) (100 mM) at pH 7.0. The different amounts of NPs were incubated in 1 mL HRP solution. The immobilization process was carried out in the cold room (4 °C) placed in a shaker [PECO pooya electronic (Mfg & Eng co)] for a specific period of time. The supernatant was then extracted by centrifuging at 7000 rpm for 7 min (BECKMAN-Avanti^{TM} 30 centrifuge). The sediments were withdrawn and rinsed for three times with PB to remove non-adsorbed enzymes. To determine the value of enzyme adsorption, the residual enzyme in the supernatant was measured using UV/visible spectroscopy (Shimadzu TCC-240A, Japan). The sediments were kept at 4 °C for further measurements.

The adsorption efficiency of enzyme onto the functionalized RGO was determined by subtracting the initial amount of enzyme from the amount of non-adsorbed enzyme in the supernatants. The concentration of non-adsorbed enzyme in the supernatant was determined by the enzyme calibration curve, and then, the amount of enzyme attached to the NPs was obtained. The enzyme adsorption efficiency was calculated by the following correlation (Xiaoche et al. 2012):

$$\text{Adsorption efficiency } \% = \frac{\text{mg of initial enzyme in buffer solution} - \text{mg of free enzyme remained in supernatant}}{\text{mg of initial enzyme in buffer solution}} \times 100.$$

Enzyme Activity Assay

The catalytic activity of the free and immobilized HRP was measured by applying a colorimetric assay. The assay solution containing 4-AAP (as chromogen), hydrogen peroxide, and phenol as substrates was used. By adding the HRP to the assay solution, the catalytic reaction was measured by the absorption of the red color product (quinone imine). The absorbency data were back-calculated to concentration using the Beer–Lambert Law with an extinction coefficient 7210 M^{-1} cm^{-1} at 510 nm (Xiaoche et al. 2012). The catalytic activities including turnover number (k_{cat}) and catalytic efficiency (k_{cat}/K_m) were determined for the free and the immobilized HRP. The data gathered from the UV/visible absorbance were adopted to the Michaelis–Menten equation. Then, the kinetic parameters (V_{max}, K_m, and k_{cat}) were obtained from the Lineweaver–Burk equation. The absorbency of HRP was measured at 403 nm to determine the enzyme concentration ($\varepsilon_{403} = 1.02 \times 10^5$ M^{-1} cm^{-1}) (Xiaoche et al. 2012).

Stabilities Measurement

The catalytic activity of the free and immobilized enzyme was investigated over a broad rang of pH values (4–11) at room temperature (25 °C). By adding hydrogen chloride and sodium hydroxide to the PB solution, the pH was

adjusted over all test runs. The thermal stability was evaluated by incubating the free and immobilized HRP at pH 7.0 and three temperatures 30, 40, and 50 °C for a specific period of time. At given time intervals, the free and immobilized HRP was taken out and kept on ice for 5 min. The residual activity was then assayed at 25 °C (Kim et al. 2009; Qiu et al. 2010). To measure the storage stability, the immobilized HRP was kept at closed containers and stored in refrigerator (4 °C) without humidity control. The enzyme activities were regularly measured one time per week during 5 weeks. The residual activity was calculated using the following correlation:

$$\text{Residual activity } (\%) = \frac{\text{The activity of the immobilized enzyme at a specified storage time}}{\text{Activity of immobilized enzyme before storage}} \times 100.$$

The Reusability Measurement

The colorimetric method was used to measure the reusability of immobilized HRP (Xiaoche et al. 2012). At the first step, the absorbency of the immobilized HRP solution was measured at 510 nm. At the second step, the sediment centrifugally separated was rinsed with the similar PB. Finally, the same amount of PB was added to sediment and the activity was measured. This procedure was repeated for ten cycles. The residual activity of the recycled HRP was compared with the initial activity of the enzyme (Temoçin and Yiğitoğlu 2009; Qiu et al. 2010; Xiaoche et al. 2012). To establish the identical condition for all test runs to compare the results, the same PB with the similar specification was used for all experiments.

Circular Dichroism (CD) Spectroscopy

The RGO·NH_2@HRP suspension (0.3 mg mL^{-1} enzyme) was collected for CD analysis (CD spectrometer, Aviv, Model-215, USA). The secondary structure of the free and immobilized enzymes was analyzed using the dedicated CD software. The far-UV region was scanned between 195 and 250 nm. The relative contents of secondary structures, including α-helix, β-sheet, β-turn, and the random coil, were calculated (Zhang et al. 2013).

Phenol Compound Measurement

The residual phenol compound in supernatant was measured by the colorimetric method using potassium ferricyanide and 4-AAP. The sample (total 1 mL) containing 1 μL of clear supernatant of the reactions was mixed with 100 μL of potassium ferricyanide (83.4 mM), 100 μL of 4-AAP (20.8 mM), and 750 μL of 0.1 M PB. When the color of the reaction mixture was completely developed with the short time, the absorbance was measured at 510 nm against a blank sample (800 μL of PB, 100 μL of potassium ferricyanide solution, and 100 μL of 4-AAP solutions). The calibration curve was drawn on the basis of standard phenol concentration with the initial reaction catalytic rate (Zhang et al. 2010). Using the calibration curve, the absorbance values were directly converted to the concentrations of phenol compound ($A_{510} = 2981.9$ [phenol], $R^2 = 0.99$).

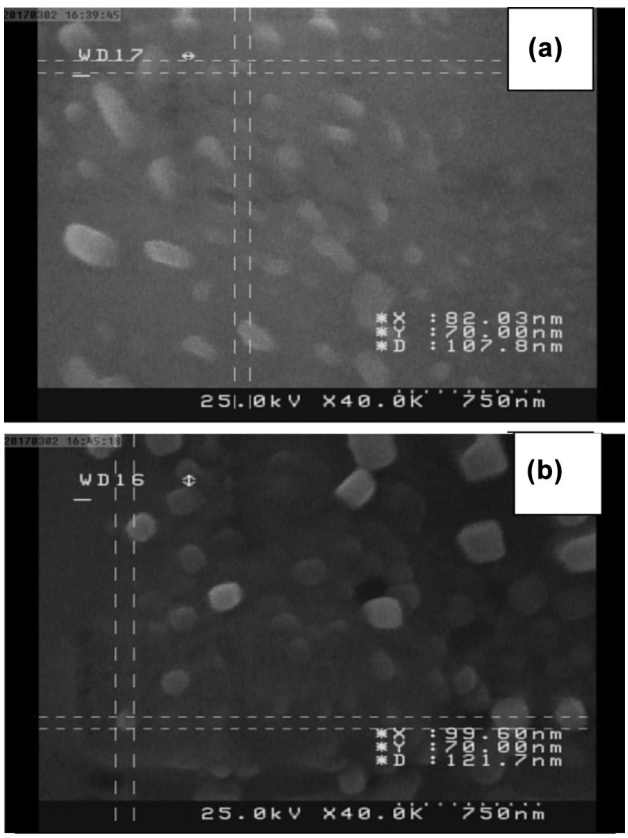

Fig. 1 SEM images: **a** RGO·NH_2 and **b** RGO·NH_2@HRP

Table 1 Surface charges of the HRP, RGO·NH_2, and RGO·NH_2@HRP

Sample	Size (nm)	Zeta potential (mV)
HRP	4.0 × 4.4 × 6.8 (Feng et al. 2015)	− 9
RGO·NH_2	70	− 17
RGO·NH_2@HRP	99	− 10

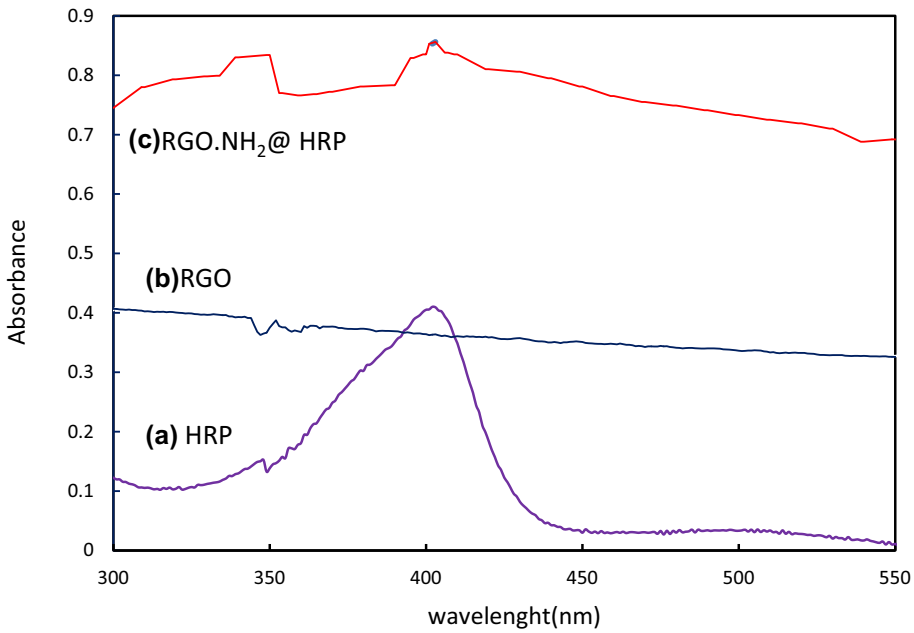

Fig. 2 UV–Vis spectrum: *a* Free HRP, *b* RGO·NH_2, and *c* RGO·NH_2@HRP at 25 °C

Results and Discussion

Characterization and Identification Analysis

The surface morphologies of the RGO·NH_2 NPs and RGO·NH_2@HRP are shown in Fig. 1. The visual observation of RGO·NH_2 and RGO·NH_2@HRP bio-nanocomposite revealed that the sizes of the NPs were about 70 and 99 nm before and after immobilization, respectively. This difference between the sizes of the NPs indicated that the enzymes were immobilized successfully on the surfaces of the NPs. The sizes measured by zeta PALS were also in fully compliance with the data obtained from the visual observation (Table 1).

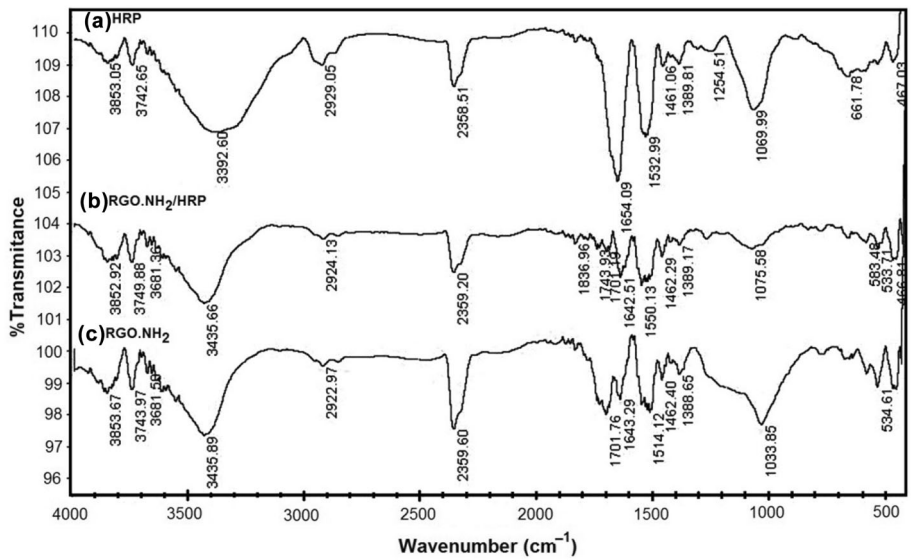

Fig. 3 FTIR spectra: *a* HRP, *b* RGO·NH_2@HRP, and *c* RGO·NH_2 NPs

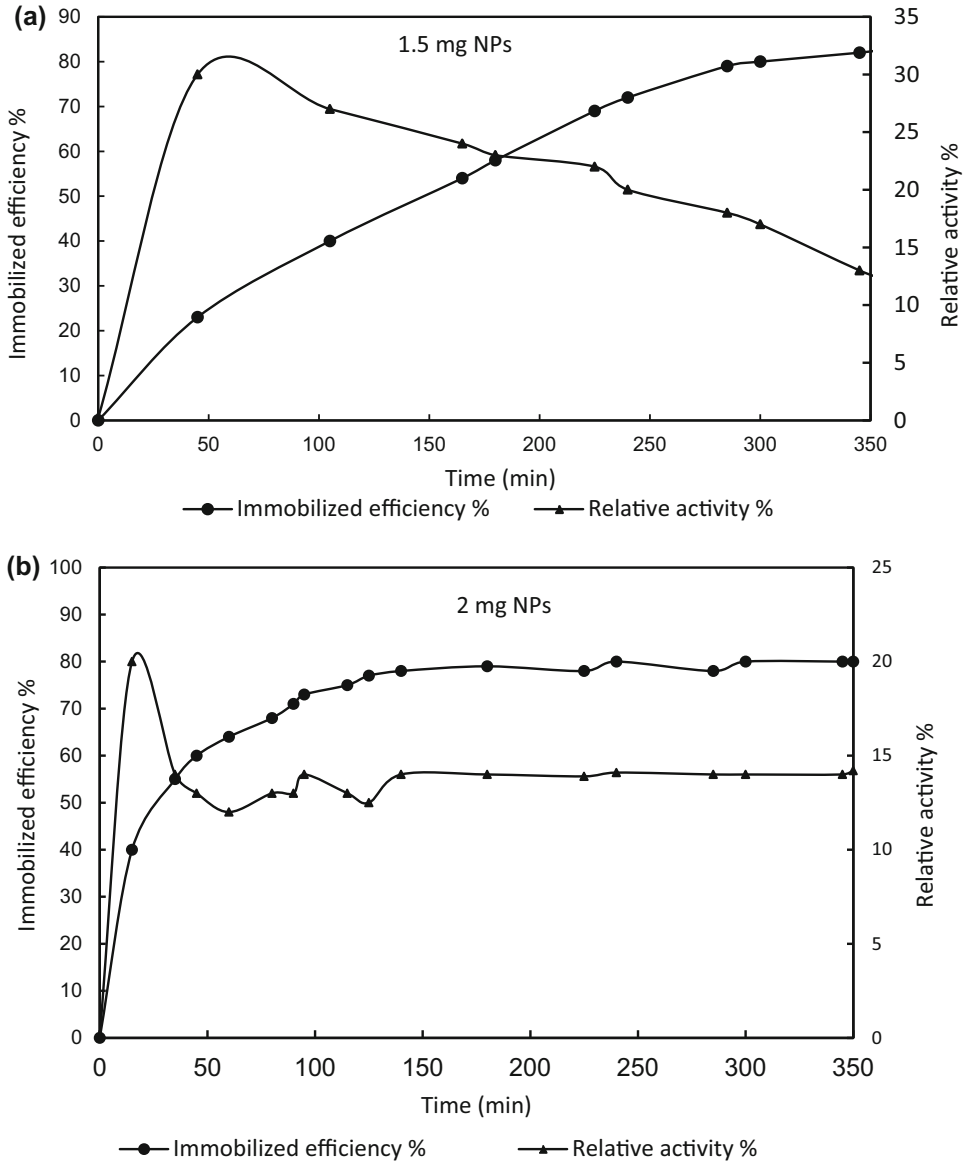

Fig. 4 Effect of the immobilization time and the relationship between the immobilized efficiency % and relative activity % for the 1.5 mg NPs (**a**) and 2 mg NPs (**b**)

The UV/visible absorption was utilized to characterize the solution of HRP stock, RGO·NH_2, and RGO·NH_2@-HRP bio-nanocomposite. The spectrum was recorded in 100 mM PB at pH 7 and 25 °C. As shown in Fig. 2a, the HRP had an absorption peak at 403 nm, attributed to the characteristic Soret band (Khavari-Nejad and Attar 2015). As compared the curve (a) for the HRP to the curve (c) for RGO·NH_2@HRP bio-nanocomposites, the similar absorption wavelength implied that the NPs did not induce significant denaturation of the HRP in PB, indicating that these NPs provided a suitable platform for the enzyme immobilization (Wang et al. 2015).

FT-IR spectra analysis was performed to identify the functional groups of HRP stock, RGO·NH_2, and RGO·NH_2@HRP. Figure 3 illustrates the FT-IR results of the obtained specimen. As shown in the FT-IR result of the free HRP, plot (a), the peaks around 1600–1700 and 1450–1600 cm^{-1} were attributed to the amides I and II, respectively. The peak around 1520 cm^{-1} was indicated to the Tyr ring stretch. The small peak around 1400 cm^{-1} was in the range of the symmetric carboxylate stretching mode (Kaposi et al. 1999). In the FT-IR result of the RGO·NH_2@HRP, plot (b), the intensity of the band in the ranges of amides, N–H bend, and C–N stretch increased, leading to adsorption of the HRP on the NPs. In plot (c) which was for FT-IR result of the RGO·NH_2, the peaks around 1530 and 1430 cm^{-1} were observed owing to N–H bend and C–N stretch, respectively.

Zeta potential (ζ) measurements were carried out to determine the surface potential at pH 7.0 and 25 °C. The data are summarized in Table 1. The zeta potential of RGO was about − 45 mV. When functionalizing the RGO by

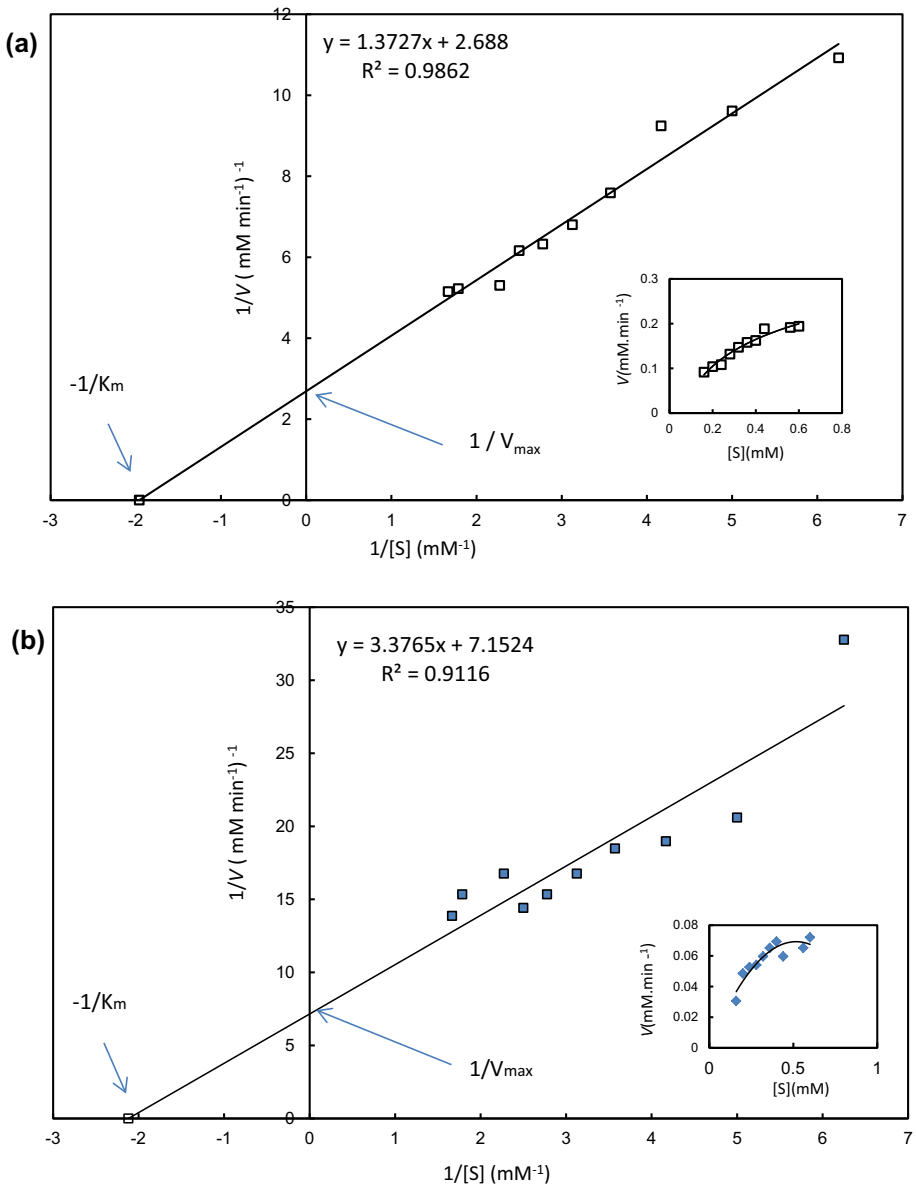

Fig. 5 Lineweaver–Burk plot for **a** free HRP and **b** immobilized HRP. The inset shows the Michaelis–Menton plot for the free and immobilized HRP

Table 2 Kinetic properties of the HRP and the RGO·NH_2@HRP

Sample	K_m (mM)	k_{cat} (s^{-1})	V_{max} (mM min^{-1})	k_{cat}/K_m (s^{-1} mM^{-1})
Free HRP	0.51 ± 0.01	560 ± 14	0.37 ± 0.001	1098
RGO·NH_2@HRP	0.47 ± 0.01	3500 ± 45	0.14 ± 0.002	7447

amino groups, the zeta potential increased to − 17 mV, resulting in reduction of the surface charges. The isoelectric pH was reported 6.6 for the free HRP (Kaszuba and Jones 1999). Because the pH was adjusted to 7.0, the zeta potential of HRP became about − 9 mV in this study. The surface charge of the free HRP reached to negative range when pH changed from 6.6 to 7.0. By immobilizing the HRP on the RGO·NH_2, the zeta potential was − 10 mV. This result indicated that immobilization of the HRP on the NPs could be able to neutralize the charge of RGO·NH_2, partially.

The zeta potential of the GO and the RGO were reported − 50 and − 30 mV, respectively (Konkena and Vasudevan 2012). They presented that the electrostatic interaction between the HRP and the GO more likely occurred with the positively charged residues on the surface of the HRP and negative charges of the GO. Zhang et al. 2010 showed that the surface of the HRP had no large positive charge fewer than ten positive charge residues. In the RGO·NH_2, the

negatively charged surface was less than the GO, so the electrostatic interaction between the free HRP and the RGO·NH_2 probably occurred through the positively charged residues (NH_3^+) on the HRP surface with negatively charged of NPs and/or a negative charge of the HRP surfaces (COO^-) with the positive charge of the NPs surfaces (NH_3^+). As a result, the RGO·NH_2 had a more electrostatic interaction with HRP as compared to the GO. By immobilizing the HRP on the RGO·NH_2, these interactions ultimately led to the negative surface charge of the RGO·NH_2@HRP bio-nanocomposite (− 10 mV).

The Relationship Between Enzyme Adsorption and Activity

In the immobilization process, it is of vital importance to obtain the actual period of reaction for process control. The large area-to-volume ratio (characteristic of a small particle size) would be a favor to enhance the catalytic activity of the enzyme. Michaelis–Menten equation could be obtained by the sequential reactions of the following equation (Segel 1993).

$$E + S \underset{k_{-1}}{\overset{k_1}{\leftrightarrow}} ES \xrightarrow{k_2} E + P. \quad (2)$$

From Eq. 2, increasing k_1 and decreasing k_{-1} improved the enzyme activity. One way to achieve this goal, the affinity between enzyme and substrate should be enhanced. In Eq. 2, the ES formation could be enhanced using the RGO because of its high affinity for the substrate. Therefore, the substrate was attracted to the enzyme physically attached to the RGO.

Figure 4 shows the adsorption efficiency and the relative activity for two amounts of the NPs with the reaction times. The maximum adsorption was obtained after 150 and 360 min of the reaction time for 2 and 1.5 mg of the NPs per 0.1 mg of the HRP, respectively. The relationship between the HRP adsorption time and the activity of the immobilized HRP is also presented in Fig. 4. As depicted, when the adsorption efficiency of the HRP was in the low level, a relatively high activity was observed. Conversely, when adsorption efficiency increased, the relative activity decreased, followed by a plateau state. It could be described that higher the HRP adsorption resulted in higher the intermolecular strict hindrance, thus limiting the complex formation of the enzyme and the substrate. This explanation was also mentioned by the previous researchers (Xiaoche et al. 2012; Zhang et al. 2010).

Kinetic Parameters

The kinetic parameters were obtained from the Lineweaver–Burk equation. Figure 5 represents the Lineweaver–Burk and Michaelis–Menton plots for the free (a) and immobilized HRP (b) at pH 7.0. Based on the intercept value of the Lineweaver–Burk plot, the kinetic parameters of K_m, V_{max} as well as k_{cat} were determined. All kinetic parameters including K_m, k_{cat}, V_{max}, and k_{cat}/K_m obtained from Fig. 5 are summarized in Table 2. When the adsorption rate of the HRP was around 60%, K_m value of the immobilized HRP (0.47 mM) was lower than that of the free HRP (0.51 mM). Therefore, the immobilized HRP provided a good affinity to the substrate. In addition, the catalytic activity of the immobilized HRP became higher as compared to the free HRP. The k_{cat} value became more than sixfold increase and the catalytic efficiency (k_{cat}/K_m) values increased about sevenfold by immobilization. All kinetic parameters such as K_m, k_{cat}, and k_{cat}/K_m improved greatly in comparison with the studies that have previously been done (Qiu et al. 2010; Xiaoche et al. 2012). The

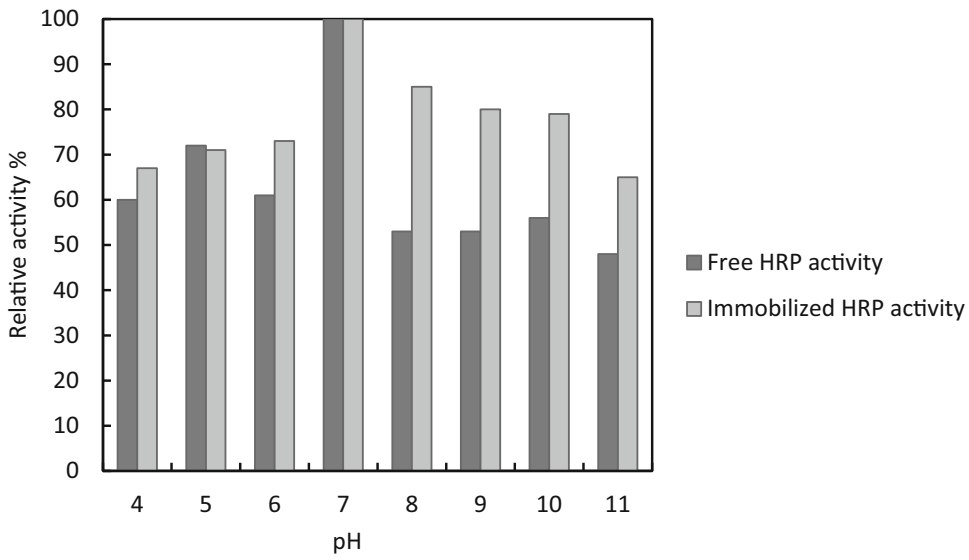

Fig. 6 Activity variation of the free and immobilized HRP against pH at 25 °C

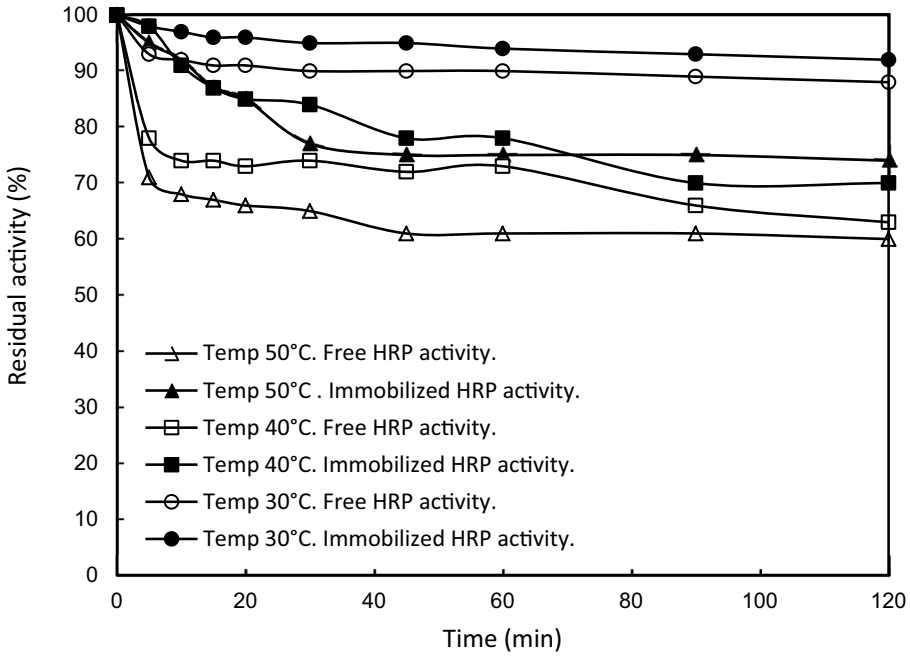

Fig. 7 Effect of temperature changes on the activities for the free and immobilized HRP

results indicated that the capability of the immobilized HRP was promoted to convert the substrates to products. The results also indicated that the RGO·NH_2 was favorable for the HRP immobilization.

pH Stability

The effect of pH variations on the activity of the free and the immobilized HRP was examined. The obtained results are illustrated in Fig. 6. The optimum pH was observed at 7.0 for the free and immobilized HRP. The results indicated that the activity of immobilized HRP was comparable to that of the free HRP, while pH was in the range of acidic conditions. In alkaline conditions, the immobilized HRP exhibited higher activity in comparison with the free HRP. The activity of the free and immobilized HRP became 53 and 85% at pH 8.0, respectively. It could be described that the RGO·NH_2 exhibited a micro-environmentally buffering effect causing the high resistance to the pH alterations in the medium, thus protecting the enzyme against the pH changes (Zhang et al. 2009; Zhou et al. 2012a). The results obtained for the pH stabilities were better as compared to the results reported by Zhang et al. (2010).

Thermal Stability

The thermal stability of the immobilized HRP on RGO·NH_2 was determined by measuring residual activities of the prepared samples incubated over different times at temperatures of 30–50 °C. To establish better benchmark, the free HRP samples were also measured in parallel under the same conditions. Figure 7 shows the residual activity variations against different temperatures with incubation time. As shown in Fig. 7, the activity of the free and the immobilized HRP decreased during the incubation for three adjusted temperatures. As illustrated in this figure, no dramatic change on the activity was observed for the free and the immobilized HRP at 30 °C after 120 min of incubation. When the incubation temperature increased to 40 and 50 °C, the immobilized HRP exhibited much higher thermal stability than the free HRP. At the incubation temperature of 50 °C, the activity of the immobilized HRP retained 75% of first activity after 120 min, while about 60% of initial activity was retained for the free HRP at the same time. A similar trend also occurred at incubation

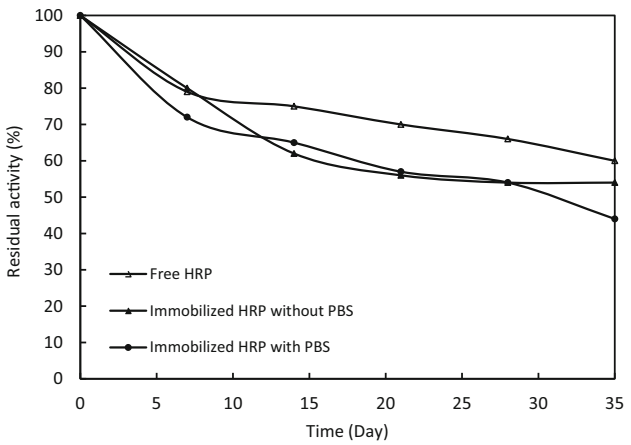

Fig. 8 Storage stability of the free and immobilized HRP at 4 °C and pH 7.0

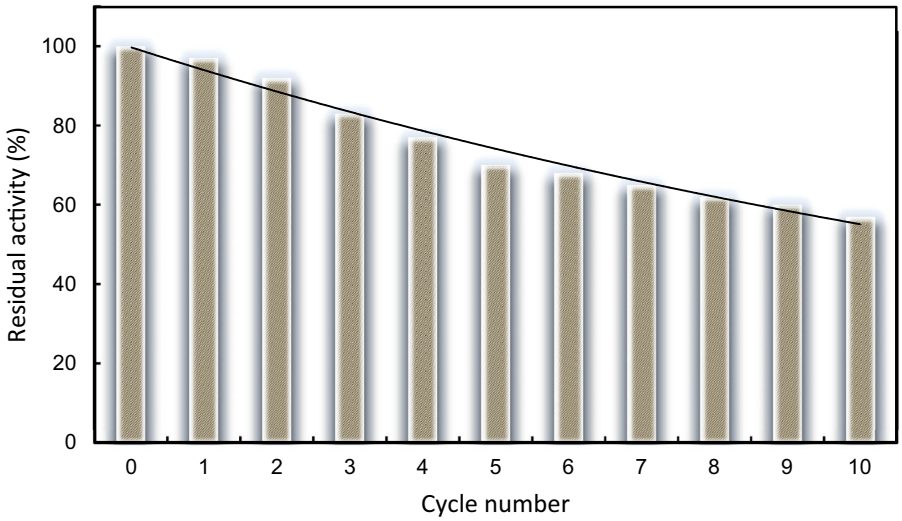

Fig. 9 Activity variation of the immobilized HRP with the number of cycles (pH 7.0, at 25 °C)

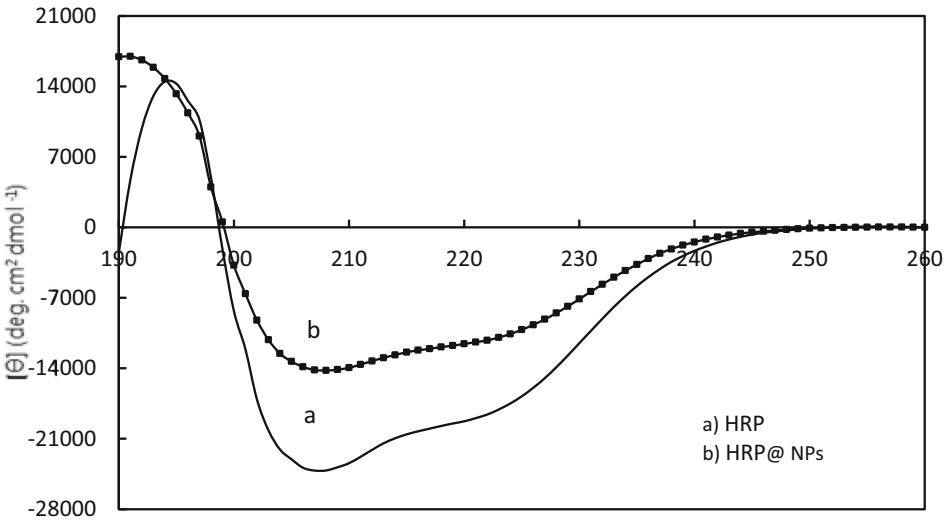

Fig. 10 CD spectra for HRP and RGO·NH_2@HRP

temperature of 40 °C. It could be concluded that the RGO·NH_2 played an effectively significant role to protect the immobilized HRP against the conformational changes possibly imposed by heating (Xu et al. 2015).

Storage Stability

To evaluate the immobilization efficiency, the storage stability of the immobilized enzyme should be considered as an important requirement (Liu et al. 2006). The storage stabilities of the free and the immobilized HRP were evaluated, and the results are presented in Fig. 8. As shown in Fig. 8, the free HRP almost 60% initial activity remained after 35-day, while the activity reached about 55% of initial activity after 35 days for the immobilized HRP. This decrease in the activities could be attributed to the conformational changes occurring during the storage period, thus hindering the formation of the catalytically active complex between active sites and substrates (Zhou et al. 2012b). The decrease in the activity was higher for the immobilized HRP than for the free HRP. It could be explained to the high tendency of the NPs to aggregate during storage period, thus leading to entrapping the HRP in the aggregated NPs.

Reusability Assay

The reusability of the immobilized enzyme can be considered as an important aspect for practical applications, especially the reuse of very expensive enzymes. In this work, the reusability was promoted greatly by introducing the functionalized NPs. As shown in Fig. 9, the relative

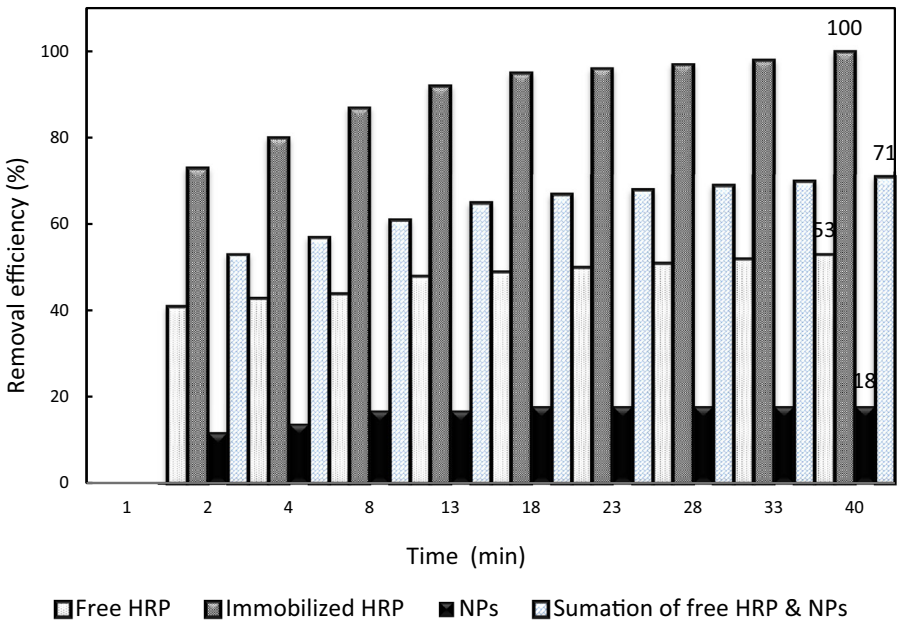

Fig. 11 Removal efficiencies of high phenol concentration (2500 mg L^{-1}) with time at 25 °C and pH 7.0

activity of the immobilized HRP decreased when the number of reuse increased subsequently. The immobilized HRP retained about 60% of initial activity after 10 cycles of reusing. Zhang et al. (2010) performed the immobilization of the HRP on the GO alone. They showed that the immobilized HRP only retained about 25% of its initial activity after 7 cycles. Qiu et al. (2010) presented that the relative activity remained 65% of the first use after 5 cycles. This reduction in the activity could be attributed to the inactivation of the enzyme caused by denaturation of the proteins and/or the enzyme leakage from the NPs surfaces over the reaction cycles. As a result, the accumulation of the products on the RGO·NH_2 during the enzymatic reaction could reduce the activity due to blockage of the active sites of the enzymes. Meanwhile, the repeated washings might disorder the electrostatic interaction; consequently, the enzymes could be desorbed from the NPs, resulting in activity reduction (Chang et al. 2015; Xu et al. 2013; Zhang et al. 2010). The number of reuse of the immobilized HRP represented a more satisfying performance as compared to the previous literatures mentioned above, which could be explained to the strong electrostatic interactions exhibited between the HRP and the NPs.

Secondary Structure Analysis

The secondary structure of the free and immobilized HRP was analyzed using the CD spectrometer. The far-UV region was scanned in the range of 195–250 nm. The contents of secondary structures such as α-helix, β-sheet, β-turn, and random coil were calculated. As shown in Fig. 10, a decrease in α-helical structure and an increase in β-sheet, β-turn, and random coil were observed due to the physical adsorption mainly occurring during the enzyme immobilization. The same trend of decrease in the α-helical content was observed in research efforts previously performed (Besharati et al. 2018; Zhang et al. 2015).

Phenol Compound Removal

The effluents coming from the industrial plants, including fiberglass, coal, iron smelting, and phenolic resins, contain high concentrations of phenol, specifically in mal-operation conditions (Basak et al. 2014; Li et al. 2006; Moussavi et al. 2010; Seid-Mohammadi et al. 2015; Zhai et al. 2012). The concentration of phenol can reach as high as 2500 mg L^{-1} in the waste streams. The efficiency of the free and immobilized HRP on RGO·NH_2 was investigated for the removal of the phenol compound with the concentration 2500 mg L^{-1}. The results are depicted in Fig. 11, where the removal efficiency was drawn against time for the free and immobilized HRP. The time for phenol degradation was set to 40 min. For free HRP, the removal efficiency finally reached 53%. This fairly low degradation of phenol could be explained to the inactivation and/or the inhibition enzyme caused by interactions between either phenoxyl radicals or phenolic polymers produced and enzymes' active sites (Gómez et al. 2006). The efficiency of the immobilized HRP reached 100% for phenol removal, resulting in no changes on the enzyme activity. Figure 11 also represents that the initial phenol degradation rate was much higher for immobilized HRP than for the free HRP. It could be attributed to the reasons, including (1) an affinity of the NPs to adsorb the phenol compound and (2) an availability of the most active sites to form the enzyme-phenol complexes. The graphs of

removal efficiency for the alone NPs and the summation of the NPs and free HRP were also obtained separately. As a result, the immobilization through physical adsorption exhibited successfully a synergetic effect between the NPs and the HRP (Besharati et al. 2018). Meanwhile, it was significant to note that short time required for biodegradation, provided that the HRP was immobilized on the NPs.

Conclusion

The systematic experiments were carried out with the free and immobilized HRP onto the RGO functionalized by amine groups and their kinetic parameters, activity, stabilities, reusability, and capacity for phenol removal were evaluated, led us to the itemized conclusions as below:

- The physical adsorption between the HRP and the functionalized RGO was performed successfully. The functionalized RGO NPs did not cause the significant denaturation of the HRP, thus providing a satisfactory platform for the immobilization. The visual observation specified the size of the functionalized RGO equalling to 70 and 99 nm before and after immobilization, respectively, which these sizes were approximately reconfirmed using zeta potential meter.
- All kinetic parameters and the catalytic activity of the HRP were greatly improved and capability of the HRP was highly promoted to convert the substrate into the product by immobilization.
- The contents of the secondary structure, including α-helix, β-sheet, β-turn, and random coil changed and a decrease in α-helical structure and an increase in β-sheet, β-turn, and random coil were concluded.
- Because of the buffering effect provided by the NPs, the immobilized HRP was less sensitive to pH changes as compared to the free HRP, resulting in the sustainable activity over the wide range of pH. Owing to the protective effect provided by the NPs, the thermostability of HRP at elevated temperatures was improved successfully after immobilization.
- The high concentration of phenol compound (2500 mg L^{-1}) was removed completely when the immobilized HRP was applied. The immobilization through physical adsorption protected effectively the HRP against inactivation during biodegradation of phenol and exhibited successfully a positively synergetic effect between the NPs and HRP.

As a complementary conclusion, the RGO·NH_2 was an excellent matrix for immobilization of HRP through physical adsorption. The immobilized enzyme system could be considered as a promising approach in wastewater treatment, biocatalysts, biosensors, and in other enzyme catalytic protocols. This system could be effectively operable and reliable, and considered as techno-economically—and eco-friendly—oriented process for large-scale application.

References

Ai J, Zhang W, Liao G, Xia H, Wang D (2016) Immobilization of horseradish peroxidase enzymes on hydrous-titanium and application for phenol removal. RSC Adv 6:38117–38123

Bansal N, Kanwar SS (2013) Peroxidase(s) in environment protection. Sci World J. https://doi.org/10.1155/2013/714639

Basak B, Bhunia B, Dutta S, Chakraborty S, Dey A (2014) Kinetics of phenol biodegradation at high concentration by a metabolically versatile isolated yeast *Candida tropicalis* PHB5. Environ Sic Pollut Res 21:1444–1454

Besharati Vineh M, Saboury AA, Poostchi AA, Rashidi AM, Parivar K (2018) Stability and activity improvement of horseradish peroxidase by covalent immobilization on functionalized reduced graphene oxide and biodegradation of high phenol concentration. Int J Biol Macromol 106:1314–1322

Chang Q, Tang H (2014) Immobilization of horseradish peroxidase on NH_2-modified magnetic Fe_3O_4/SiO_2 particles and Its application in removal of 2,4-dichlorophe. Molecules 19:15768–15782

Chang Q, Jiang G, Tang H, Lia N, Huang J, Wu L (2015) Enzymatic removal of chlorophenols using horseradish peroxidase immobilized on superparamagnetic Fe_3O_4/graphene oxide nanocomposite. Chin J Catal 36:961–968

Chang Q, Huang J, Ding Y, Tang H (2016) Catalytic oxidation of phenol and 2,4-dichlorophenol by using horseradish peroxidase immobilized on graphene oxide/Fe_3O_4. Molecules 21(8):1044. https://doi.org/10.3390/molecules21081044

Dahili LA, Kelemen-Horváth I, Feczkó T (2015) 2,4-dichlorophenol removal by purified horseradish peroxidase enzyme and crude extract from horseradish immobilized to nano spray dried ethyl cellulose particles. Process Biochem 50:1835–1842

Feng D, Liu T-F, Su J, Bosch M, Wei Z, Wan W, Yung D, Chen YP, Wang X, Wang K, Lian X, Yuan Gu Z, Zou JPX, Zhou H-C (2015) Stable metal-organic frameworks containing single-molecule traps for enzyme encapsulation. Nat Commun 6 Article number: 5979

Gómez JA, Bódalo A, Gómez E, Bastida J, Gómez M (2006) Immobilization of peroxidases on glass beads: an improved alternative for phenol removal. Enz Microb Technol 39:1016–1022

Guo X, Mei N (2014) Assessment of the toxic potential of graphene-family nanomaterials. J Food Drug Anal 22:105–115

Kaposi AD, Fidy J, Manas ES, Vanderkooi JM, Wright WW (1999) Horseradish peroxidase monitored by infrared spectroscopy: effect of temperature, substrate and calcium. Biochim Biophys Acta 1435:41–50

Kaszuba M, Jones MN (1999) Hydrogen peroxide production from reactive liposomes encapsulating enzymes. Biophys Acta 1419:221–228

Kemp KC, Seem H, Saleh M, Le NH, Mahesh K, Chandra V, Kim KS (2013) Environmental applications using graphene composites: water remediation and gas adsorption. Nanoscale 5:3149–3171

Khavari-Nejad S, Attar F (2015) In Vitro study of acriflavine interaction with horseradish peroxidase C. Biomacromol J 1:130–139

Khurshid S, Qureshi MZ, Ibrahim A, Nawaz Z, Ikram AS (2012) Production and purification of horseradish peroxidase in Pakistan. Int J Phys Sci 7:2706–2712

Kim BJ, Kang BK, Bahk YY, Yoo KH, Lim KJ (2009) Immobilization of horseradish peroxidase on multi-walled carbon nanotubes and its enzymatic stability. Curr Appl Phys 9:e263–e265

Konkena B, Vasudevan S (2012) Understanding aqueous dispersibility of graphene oxide and reduced graphene oxide through pKa measurements. J Phys Chem Lett 3:867–872

Lavery CB, MacInnis MC, MacDonald MJ, Williams JB, Spencer CA, Burke AA, Irwin DJG, D'Cunha GB (2010) Purification of peroxidase from horseradish (*Armoracia rusticana*) Roots. J Agric Food Chem 58:8471–8476

Li X, Wang T, Sun J, Huang X, Kong X (2006) Biodegradation of high concentration phenol containing heavy metal ions by functional biofilm in bioelectro-reactor. J Environ Sci (China) 18:639–643

Liu Z-M, Tingry S, Innocent C, Durand J, Xu Z-K, Seta P (2006) Modification of microfiltration polypropylene membranes by allylamine plasma treatment Influence of the attachment route on peroxidase immobilization and enzyme efficiency. Enzyme Microb Technol 39:868–876

Mogharrab N, Ghourchian H, Amininasab M (2007) Structural stabilization and functional improvement of horseradish peroxidase upon modification of accessible lysines: experiments and simulation. Biophys J 92:1192–1203

Moussavi G, Barikbin B, Mahmoudi M (2010) The removal of high concentrations of phenol from saline wastewater using aerobic granular SBR. Chem Eng J 158:498–504

Pradeep NV, Anupam S, Navya K, Shalini HN, Hampannavar M, Idris US (2015) Biological removal of phenol from wastewaters: a mini review. Appl Water Sci 5:105–112

Qiu H, Lu L, Huang X (2010) Immobilization of horseradish peroxidase on nanoporous copper and its potential applications. Bioresour Technol 101:9415–9420

Segel IH (1993) Enzyme kinetics: behavior and analysis of rapid equilibrium and steady-state enzyme systems. Wiley, New York

Seid-Mohammadi A, Asgari G, Poormohammadi A, Ahmadian M, Rezaeivahidian H (2015) Removal of phenol at high concentrations using UV/Persulfate from saline wastewater. Desalin Water Treat 57(42):19988–19995. https://doi.org/10.1080/19443994.2015.1102770

Sun D, Cai C, Li X, Xing W, Lu T (2004) Direct electrochemistry and bioelectrocatalysis of horseradish peroxidase immobilized on active carbon. J Electroanal Chem 566:415–421

Tavakoli F, Badiei A, Ziarani GM, Tarighi S (2017) Photocatalytic application of TiO_2–AgI hybrid for degradation of organic pollutants in water. Int J Environ Res 11:217–224

Temoçin Z, Yiğitoğlu M (2009) Studies on the activity and stability of immobilized horseradish peroxidase on poly(ethylene terephthalate) grafted acrylamide fiber. Bioprocess Biosyst Eng 32:467–474

Wang Y, Wang Z, Rui Y, Li M (2015) Horseradish peroxidase immobilization on carbon nanodots/CoFe layered double hydroxides: direct electrochemistry and hydrogen peroxodase sensing. Biosens Bioelectron 64:57–62

Xiaoche W, Yan Z, Congyu W, Haixia W (2012) Preparation and characterization of magnetic Fe_3O_4/CRGO nanocomposites for enzyme immobilization. Trans Nonferrous Met Soc China 22:s162–s168

Xu R, Chi C, Li F, Zhang B (2013) Immobilization of horseradish peroxidase on electrospun microfibrous membranes for biodegradation and adsorption of bisphenol A. Bioresour Technol 149:111–116

Xu R, Si Y, Li F, Zhang B (2015) Enzymatic removal of paracetamol from aqueous phase: horseradish peroxidase immobilized on nanofibrous membranes. Environ Sci Pollut Res 22:3838–3846

Zhai Z, Wang H, Yan S, Yao J (2012) Biodegradation of phenol at high concentration by a novel bacterium: *Gulosibacter* sp. YZ4. J Chem Technol Biotechnol 87:105–111

Zhai R, Zhang B, Wan Y, Li C, Wang J, Liu J (2013) Chitosan–halloysite hybrid-nanotubes: horseradish peroxidase immobilization and applications in phenol removal. Chem Eng J 214:304–309

Zhang Y, Hong W, Lin I, Jian L, Zhongyi J, Yanjun J, Ying C (2009) Enzymatic conversion of Baicalin into Baicalein by _glucuronidase encapsulated in biomimetic core-shell structured hybrid capsules. J Mol Catal B Enzyme 57:130–135

Zhang F, Zheng B, Zhang J, Huang X, Liu H, Guo S, Zhang J (2010) Horseradish peroxidase immobilized on graphene oxide: physical properties and applications in phenolic compound removal. J Phys Chem C 114:8469–8473

Zhang Y, Wu C, Guo S, Zhang J (2013) Interactions of graphene and graphene oxide with proteins and peptides. Nanotechnol Rev 2:27–45

Zhang T, Xu X-L, Jin Y-N, Wu J, Xu Z-K (2014) Immobilization of horseradish peroxidase (HRP) on polyimide nanofibers blending with carbon nanotubes. J Mol Catal B Enzyme 106:56–62

Zhang CD, Chen S, Alvarez PJJ, Chen W (2015) Reduced graphene oxide enhances horseradish peroxidase stability by serving as radical scavenger and redox mediator. Carbon 94:531–538

Zhou L, Jiang Y, Gao J, Zhao X, Ma L, Zhou G (2012a) Oriented immobilization of glucose oxidase on graphene oxide. Biochem Eng J 69:28–31

Zhou L, Jiang Y, Gao J (2012b) Graphene oxide as a matrix for the immobilization of glucose oxidase. Appl Biochem Biotechnol 168:1635–1642